Spurious finite-size instabilities in nuclear energy density functionals

V. Hellemans,[1,*] A. Pastore,[2,3,4,†] T. Duguet,[5,6] K. Bennaceur,[3,4,7] D. Davesne,[3,4] J. Meyer,[3,4] M. Bender,[8,9] and P.-H. Heenen[1]

[1]*PNTPM, CP229, Université Libre de Bruxelles, B-1050 Bruxelles, Belgium*

[2]*IAA, CP226, Université Libre de Bruxelles, B-1050 Bruxelles, Belgium*

[3]*Université Lyon 1, 43 Boulevard du 11 Novembre 1918, F-69622 Villeurbanne cedex, France*

[4]*CNRS-IN2P3, UMR 5822, Institut de Physique Nucléaire de Lyon, 4 Rue Enrico Fermi, 69622 Villeurbanne Cedex, France*

[5]*CEA-Saclay DSM/IRFU/SPhN, F-91191 Gif sur Yvette Cedex, France*

[6]*National Superconducting Cyclotron Laboratory and Department of Physics and Astronomy, Michigan State University, East Lansing, Michigan 48824, USA*

[7]*Department of Physics, P.O. Box 35 (YFL), Fl-40014 University of Jyväskylä, Finland*

[8]*Université Bordeaux, Centre d'Etudes Nucléaires de Bordeaux Gradignan, UMR5797, F-33170 Gradignan, France*

[9]*CNRS/IN2P3, Centre d'Etudes Nucléaires de Bordeaux Gradignan, UMR5797, F-33170 Gradignan, France*

(Received 30 October 2013; revised manuscript received 28 November 2013; published 23 December 2013)

Background: It is known that some well established parametrizations of the nuclear energy density functional (EDF) do not always lead to converged results for nuclei. Earlier studies point towards the existence of a qualitative link between this finding and the appearance of finite-size instabilities of symmetric nuclear matter (SNM) near saturation density when computed within the random phase approximation (RPA).

Purpose: We aim to establish a stability criterion based on computationally friendly RPA calculations that can be incorporated into fitting procedures of the coupling constants of the EDF. Therefore, a quantitative and systematic connection between the impossibility to converge self-consistent calculations of nuclei and the occurrence of finite-size instabilities in SNM is investigated for the scalar-isovector ($S = 0$, $T = 1$) instability of the standard Skyrme EDF.

Results: Tuning the coupling constant $C_1^{\rho\Delta\rho}$ of the gradient term that triggers scalar-isovector instabilities of the standard Skyrme EDF, we find that the occurrence of instabilities in finite nuclei depends strongly on the numerical scheme used to solve the self-consistent mean-field equations. Once the critical value of the coupling constant $C_1^{\rho\Delta\rho}$ is determined in nuclei, one can extract the corresponding lowest density $\rho_{\rm crit}$ at which a pole appears at zero energy in the RPA response function.

Conclusions: Instabilities of finite nuclei can be artificially hidden due to the choice of inappropriate numerical schemes or overly restrictive, e.g., spherical, symmetries. Our analysis suggests a twofold stability criterion to avoid scalar-isovector instabilities.

DOI: 10.1103/PhysRevC.88.064323 PACS number(s): 21.30.Fe, 21.60.Jz, 21.65.−f, 31.15.E−

I. INTRODUCTION

Energy density functionals (EDFs) are popular tools for the description of fermionic systems within self-consistent mean-field methods and are successfully applied to describe atomic nuclei [1], liquid helium [2,3], helium droplets [4,5], and cold atoms in traps [6]. A phenomenological approach is usually adopted and the parameters of the EDF are adjusted to selected properties of finite and idealized infinite systems, such as electron gas or homogeneous nuclear matter. However, the possibility that such a parametrization gives rise to unphysical behavior cannot be discarded. Indeed, the example discussed in the present paper manifests itself by the impossibility to converge the iterative procedure to solve the mean-field equations for the ground states of some nuclei (e.g., see Refs. [7–10]). Such nonconvergence is a fingerprint of an instability that can be characterized in the idealized system of homogeneous isospin-symmetric nuclear matter (SNM). Two cases must be distinguished.

First, Landau-Migdal parameters [11] can guide the identification of instabilities in the infinite-wavelength limit (or zero-momentum transfer $q_{\rm ph} = 0$) of the response function. Such instabilities are characterized by the transition between two different homogeneous phases of SNM [12]. Since state-of-the-art *ab initio* many-body calculations predict SNM to be stable in all spin-isospin channels up to several times saturation density [13,14], the Landau-Migdal parameters are often used to validate or even constrain the parameters of the EDF.

Second, more general *finite-size* instabilities may appear at finite momentum transfer $q_{\rm ph} \neq 0$ [8]. A scan of the linear response to a perturbation in each of the four spin-isospin (S,T) channels of the particle-hole interaction can identify such instabilities at a given density and wavelength (or, equivalently, transferred momentum $q_{\rm ph}$). The necessary tools for such studies have been developed for nonrelativistic Skyrme parametrizations of the nuclear EDF [8,15–18]. Typically, the instability arises as a collective mode at zero excitation energy, signaling the transition of homogeneous matter to an inhomogeneous phase. The only known *physical* example of such a finite-size instability of homogeneous matter is the so-called spinodal instability in the $S = 0, T = 0$ channel [18–21], which sets in below about 2/3 of nuclear saturation density

*vhellema@ulb.ac.be

†apastore@ulb.ac.be

in SNM. Then, homogeneous nuclear matter becomes unstable against the formation of finite-size clusters. To the best of our knowledge, no *ab initio* prediction exists regarding the stability of SNM with respect to finite-wavelength perturbations in the three other spin-isospin channels. However, as we shall see below, the very existence of nuclei excludes the possibility of finite-size instabilities of homogeneous matter for a wide range of densities and transferred momenta.

Several investigations of finite-size instabilities have been undertaken [8–10,22–25] thus far. However, a systematic analysis of the connection between the impossibility to converge self-consistent calculations of nuclei and the occurrence of finite-size instabilities in SNM is still lacking. Such a relationship is not straightforward as nuclei are affected by shell and surface effects that do not occur in SNM. In the present paper, we seek to establish a transparent, that is, a quantitative and systematic correspondence, irrespective of the details of the EDF parametrization. We will concentrate on scalar-isovector ($S = 0, T = 1$) instabilities using the standard form of the EDF, as obtained from the density-dependent two-body Skyrme force [1]. These instabilities are induced by a strongly attractive scalar-isovector gradient term of the form

$$E_1^{\rho\Delta\rho} \equiv \int d^3\mathbf{r}\, \mathcal{E}_1^{\rho\Delta\rho}(\mathbf{r}) \equiv \int d^3\mathbf{r}\, C_1^{\rho\Delta\rho}\, \rho_1(\mathbf{r})\, \Delta\rho_1(\mathbf{r}). \quad (1)$$

and manifest themselves as unphysical strong oscillations of the scalar-isovector density $\rho_1(\mathbf{r}) \equiv \rho_n(\mathbf{r}) - \rho_p(\mathbf{r})$ that measures the local difference between neutron and proton matter density distributions [7,8]. Instabilities triggered by terms containing gradients of spin densities have been encountered as well [9,10,26] but are not included in the present analysis. Finally, if a one-to-one correspondence between instabilities in finite nuclei and SNM can be established, we wish to introduce a criterion based on computationally friendly random-phase approximation (RPA) calculations of SNM to control the stability of EDF parametrization during the adjustment of its coupling constants.

The paper is organized as follows. In Sec. II, we introduce the protocol of our analysis and detail the methods used. The results obtained with this protocol are presented and analyzed in Sec. III. Conclusions are given in Sec. IV.

II. PROTOCOL OF THE ANALYSIS

A. Procedure

The present analysis is carried out for nine parametrizations that are all based on the traditional form [1] of the Skyrme EDF. Four of the selected parametrizations (KDE0v1, LNS, NRAPRii,[1] and SQMC700) were recently shown to be consistent with a large set of pseudodata in SNM [28] and were adjusted to no or a very limited number of nuclear masses. The remaining five, SkM*, SLy5, T11, T44, and UNEDF0, were adjusted to selected properties of finite nuclei and SNM and are widely used. Basic SNM properties of each parametrization are summarized in Table I.

TABLE I. Basic SNM properties for the nine Skyrme parametrizations used in the present work.

Param.	Ref.	m_s^*/m	m_v^*/m	$\rho_{\rm sat}$	K_∞	$a_{\rm sym}$
KDE0v1	[29]	0.74	0.81	0.165	227	34.6
LNS	[30]	0.83	0.73	0.175	211	33.4
NRAPRii	[31]	0.69	0.60	0.161	226	32.8
SQMC700	[32]	0.76	0.64	0.170	220	43.5
SkM*	[33]	0.79	0.65	0.160	217	30.0
SLy5	[34]	0.70	0.80	0.160	230	32.0
T11	[35]	0.70	0.80	0.161	230	32.0
T44	[35]	0.70	0.80	0.161	230	32.0
UNEDF0	[36]	1.11	0.80	0.161	230	30.5

As mentioned before, the instability under study is triggered by the term $E_1^{\rho\Delta\rho}$ and can be controlled with the coupling constant $C_1^{\rho\Delta\rho}$ if one uses the standard form of the Skyrme EDF. Although the protocol to adjust the coupling constants of the EDF strongly differs for the nine parametrizations, the scalar-isovector instabilities arise at a rather universal critical value of $C_1^{\rho\Delta\rho}$, as will be discussed later on. However, in anticipation of the future use of more elaborate EDFs [37–39] for which the finite-size instability in a given (S,T) channel may be related to several terms in the energy density, it is preferable to associate the instability with a *physical* quantity rather than a coupling constant.

Such a connection can be established by means of RPA calculations of SNM. Within this approach, the instability of the density is marked by the occurrence of a pole at $\omega = 0$ and finite momentum in the response function $\chi_{\rm RPA}^{(S,T)}(q_{\rm ph},\omega;k_F)$; that is, by the existence of a zero-energy excitation mode. The solution of this implicit equation determines domains of instability in the $(q_{\rm ph},k_F)$ plane whose boundaries define the curve $\rho_p(q_{\rm ph})$, where $\rho \equiv 2k_{\rm F}^3/3\pi^2$. For the central terms of the Skyrme EDF, the formalism to compute $\chi_{\rm RPA}^{S,T}(q_{\rm ph},\omega;k_F)$ is outlined in Ref. [15] and the extension to spin-orbit and tensor terms can be found in Refs. [16] and [17,18], respectively. In Ref. [18], it was also shown that the extraction of unstable modes at density ρ and momentum transfer $q_{\rm ph}$ can be efficiently performed on the basis of the inverse energy-weighted sum rule.

The analysis is performed in three steps:

(1) For each of the nine parametrizations, the value of $C_1^{\rho\Delta\rho}$ is increased from its nominal value up to a critical value leading to nonconvergence in steps of 0.1 MeV fm^5. In the following, such an alteration of the original parametrization is indicated with a prime (as SLy5′). We have verified that the variation of $C_1^{\rho\Delta\rho}$ around its nominal value does not significantly deteriorate the overall properties of the parametrization [40].

(2) Such a modified parametrization should be discarded if it leads to nonconvergence in the calculation of the ground-state energy of any finite nucleus. For reasons of numerical manageability, we chose a representative

[1]The notation ii indicates that we have doubled the strength W_0 of the spin-orbit interaction of the original NRAPR parametrization, as suggested in [27].

set of nine spherical doubly closed-shell nuclei (^{16}O, ^{40,48}Ca, ^{56,78}Ni, ^{100,132,176}Sn, ^{208}Pb) and one well-deformed open-shell nucleus (^{170}Hf) to investigate the effect of deformation. For even-even nuclei, time-reversal symmetry can be enforced and suppresses possible spin ($S=1$) instabilities originating from time-odd terms of the EDF. Also, pairing correlations are neglected. For each of the nine parametrizations, the critical value $C_{1,\mathrm{crit}}^{\rho\Delta\rho}$ is defined as the smallest value of $C_1^{\rho\Delta\rho}$ at which an instability occurs in any of the selected nuclei.

(3) Finally, we extract the minimum of $\rho_p(q_{\mathrm{ph}})$, referred to as ρ_{crit}, for $C_1^{\rho\Delta\rho} = C_{1,\mathrm{crit}}^{\rho\Delta\rho}$ and analyze whether it displays a universal value.

As will be discussed in Sec. III, the density distribution of ^{40}Ca exhibits a central bump of about $1.2\rho_{\mathrm{sat}}$, making this nucleus particularly prone to instabilities. To facilitate the further analysis of the results of steps 2 and 3 in our protocol, we therefore introduce the scalar-isoscalar density at the center of ^{40}Ca, $\rho_{\mathrm{cent}} = \rho_0(\mathbf{0})$, and the relative momentum distribution at $\mathbf{R} = \mathbf{0}$ through

$$f_i(\mathbf{q}) = \frac{1}{(2\pi)^{3/2}} \int e^{-i\mathbf{q}\cdot\mathbf{s}} \rho_i(\mathbf{0},\mathbf{s})\, d^3s, \tag{2}$$

where $\rho_i(\mathbf{R},\mathbf{s})$ is the nonlocal scalar density for species $i = n$ or p as a function of the center-of-mass and relative coordinates $\mathbf{R}$ and $\mathbf{s}$. This definition of $f_i(\mathbf{q})$ is different from the one used in [41] and allows one to recover the central density through

$$\rho_i(\mathbf{0},\mathbf{0}) = \frac{1}{(2\pi)^{3/2}} \int f_i(\mathbf{q})\, d^3\mathbf{q}. \tag{3}$$

B. Numerical detections of instabilities

Preliminary inquiries suggested that the detection of instabilities in nuclei depends on the numerical algorithm, on the symmetry restrictions imposed to solve the equations, and on the accuracy required. To investigate such features and limit the numerical bias, we therefore performed the analysis with three methods, two of which imposing spherical symmetry.

(1) In HOSPHE [42], single-particle wave functions are expanded on an optimized spherical harmonic oscillator (HO) basis. The accuracy is varied by changing the number of shells N_{sh} in the HO basis.

(2) In LENTEUR [43], one-body equations are solved in coordinate space enforcing spherical symmetry. Radial wave functions with an angular momentum up to $41/2\,\hbar$ are discretized on a mesh along a radius of 18 fm. Decreasing the step size dr of the radial mesh increases the accuracy of the calculation.

(3) In EV8 [44], single-particle wave functions are discretized on a three-dimensional (3D) Cartesian mesh. Three symmetry planes are imposed, corresponding to the description of triaxially deformed shapes. The accuracy of the calculation can be changed by means of the step size dx of the mesh.

III. RESULTS

A. Analysis in nuclei

Here, we carry out steps 1 and 2 of the protocol described in Sec. II B.

1. Detection of finite-size instabilities within different numerical schemes

As the one-body equations of motion are solved iteratively, an instability in the $S = 0$, $T = 1$ channel occurs when it becomes energetically favorable to build oscillations of neutrons against protons of unlimited amplitude [8]. In a code based on an oscillator-basis expansion such as HOSPHE, this manifests itself differently than in codes using a discretization on a 1D or a 3D mesh. Indeed, for LENTEUR, the calculation is halted when density oscillations make the isovector gradient term unreasonably large, whereas for EV8 the convergence criteria are never reached. This permits a clear determination of the instability at all accuracies. By contrast, the detection of $C_{1,\mathrm{crit}}^{\rho\Delta\rho}$ is less obvious with HOSPHE. Figure 1 illustrates this for the $N = Z$ nucleus ^{40}Ca and for ^{208}Pb. The binding energy is plotted as a function of $C_1^{\rho\Delta\rho}$ for different choices of the number of oscillator shells N_{sh}. For both nuclei, the energy decreases up to a value of $C_1^{\rho\Delta\rho}$ where the convergence criteria on energy cannot be met in spite of an unusually large number of iterations (up to 40 000 in our calculations). For small N_{sh} ($N_{\mathrm{sh}} \leqslant 40$ for ^{40}Ca and $N_{\mathrm{sh}} \leqslant 50$ for ^{208}Pb), one obtains an apparent convergence for values of $C_1^{\rho\Delta\rho}$ in the vicinity of $C_{1,\mathrm{crit}}^{\rho\Delta\rho}$ but with an unphysical large value of the binding energy, indicating that the instability in fact occurs already at smaller values of $C_1^{\rho\Delta\rho}$. In ^{40}Ca, a 1 MeV fm^5 increase of $C_1^{\rho\Delta\rho}$ leads to a change in total energy of the order of tens of keV for $N_{\mathrm{sh}} = 20$ and of tens of MeV for $N_{\mathrm{sh}} = 30,40$ in that region of the plot. These numbers have

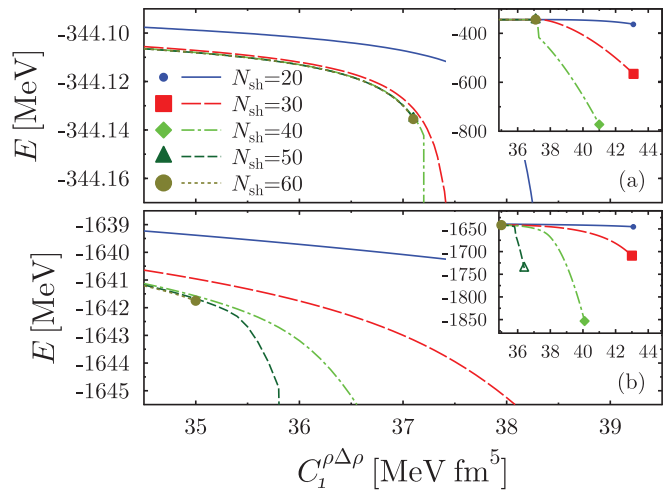

FIG. 1. (Color online) Binding energy of (a) ^{40}Ca and (b) ^{208}Pb obtained from HOSPHE and SLy5′ [34] as a function of $C_1^{\rho\Delta\rho}$. Calculations are performed for several values of the number of shells N_{sh}. The curves end at the largest value of $C_1^{\rho\Delta\rho}$ for which the convergence criteria are reached within 40 000 iterations.

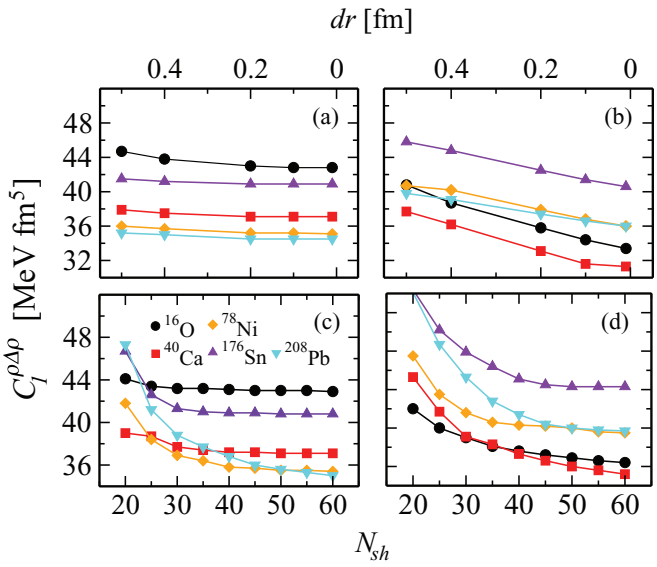

FIG. 2. (Color online) Maximum value of $C_1^{\rho\Delta\rho}$ for which a solution is found for the ground state of a given nucleus. Results are displayed for SLy5′ [(a) and (c)] and LNS′ [(b) and (d)]. Results are displayed in the upper (lower) panel as a function of the mesh (basis) size used in LENTEUR (HOSPHE).

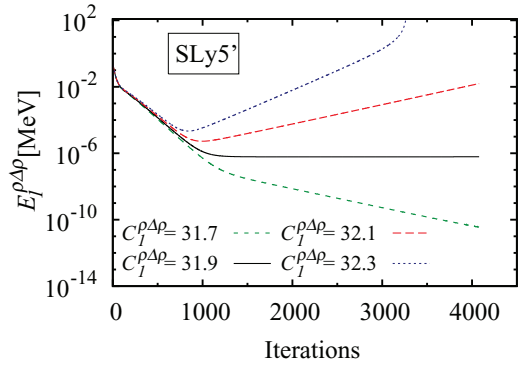

FIG. 3. (Color online) Contribution of $E_1^{\rho\Delta\rho}$ to the binding energy of ^{40}Ca as a function of the number of iterations. Four modified SLy5′ [34] parametrizations with values of $C_1^{\rho\Delta\rho}$ around its critical value $C_{1,\mathrm{crit}}^{\rho\Delta\rho}$ are represented. Calculations are performed with the EV8 code for a value $dx = 0.4$ fm of the Cartesian mesh. During the iterations, the Coulomb term in the EDF is switched off, such that the exact value of $E_1^{\rho\Delta\rho}$ should be zero for ^{40}Ca.

to be compared with those of EV8 where, for all mesh sizes, the energy only varies by a few keV for a 1 MeV fm^5 step in $C_1^{\rho\Delta\rho}$ below $C_{1,\mathrm{crit}}^{\rho\Delta\rho}$. Increasing N_{sh} to unusually large values makes the detection of instabilities easier, but still leads to values of $C_{1,\mathrm{crit}}^{\rho\Delta\rho}$ significantly larger than those found with LENTEUR and EV8, even for $N_{\mathrm{sh}} = 60$. This result clearly illustrates the shortcomings of an oscillator basis for the accurate determination of $C_{1,\mathrm{crit}}^{\rho\Delta\rho}$. It also demonstrates that the manifestation of finite-size instabilities can be obscured by a choice of N_{sh} leading to an apparent convergence of the binding energies but artificially suppressing the instability.

2. *Determination of instabilities with the spherical codes*

Systematic calculations with both HOSPHE and LENTEUR for ^{16}O, ^{40,48}Ca, ^{56,78}Ni, ^{100,132,176}Sn, and ^{208}Pb have shown that the lowest $C_1^{\rho\Delta\rho}$ at which the instability sets in is always found for either ^{40}Ca or ^{208}Pb. This is illustrated in Fig. 2 for ^{16}O, ^{40}Ca, ^{78}Ni, ^{176}Sn, and ^{208}Pb with SLy5′ and LNS′. Results for ^{56}Ni and ^{100,132}Sn were omitted for reasons of presentation but are in all cases situated between the lowest and highest curves. For LNS′, the critical value of $C_1^{\rho\Delta\rho}$ is obtained in ^{40}Ca whereas for SLy5′ it is found in ^{208}Pb. In the latter case, several nuclei lead to similar values. Throughout our analysis and at the highest accuracy of the two spherical codes, the lowest values of $C_{1,\mathrm{crit}}^{\rho\Delta\rho}$ are systematically obtained with LENTEUR.

3. *Determination of instabilities with the 3D code*

Because the calculations with the 3D code are very time consuming at small mesh sizes, they were limited to these two doubly-magic nuclei and a deformed one, ^{170}Hf, and $C_1^{\rho\Delta\rho}$ was initially varied in steps of 1 MeV fm^5. Results with LENTEUR and EV8 are consistent but $C_{1,\mathrm{crit}}^{\rho\Delta\rho}$ systematically takes lower values with EV8, as can be seen for example by comparing Figs. 2 and 4. This can be explained by the lower degree of symmetry of the latter code, which allows more freedom to develop oscillations in a "spherical" nucleus. Our observation that ^{170}Hf and ^{208}Pb give rise to almost identical $C_{1,\mathrm{crit}}^{\rho\Delta\rho}$ can be understood from this argument. For all parametrizations studied with EV8, the value of $C_1^{\rho\Delta\rho}$ at which the instability sets in is systematically the lowest in ^{40}Ca. Therefore, in the following, we concentrate on the results obtained with EV8 for ^{40}Ca. At $dx = 0.40$ fm, the size of the box in all directions was chosen equal to 26 fm and for larger values of dx the number of points on the mesh was adjusted accordingly.

In a next step, we compute the energy of ^{40}Ca without Coulomb interaction to obtain an accurate determination of $C_{1,\mathrm{crit}}^{\rho\Delta\rho}$ up to a precision of 0.1 MeV fm^5. Indeed, ^{40}Ca being an $N = Z$ nucleus, $E_1^{\rho\Delta\rho}$ should be zero at convergence. The starting point of the iterations is a converged wave function of

TABLE II. Nominal values of $C_1^{\rho\Delta\rho}$ (MeV fm^5). The critical coupling constant $C_{1,\mathrm{crit}}^{\rho\Delta\rho}$ is obtained for ^{40}Ca with EV8 and $dx = 0.4$ fm. The $\rho_{\mathrm{min}}/\rho_{\mathrm{sat}}$ and $\rho_{\mathrm{crit}}/\rho_{\mathrm{sat}}$ are extracted from Figs. 7 and 8, respectively. Values indicated with a star (*) are extracted from the asymptotic behavior of $\rho_p(q_{\mathrm{ph}})$ (see Sec. III B for more details).

Param.	Ref.	$C_1^{\rho\Delta\rho}$	$\rho_{\mathrm{min}}/\rho_{\mathrm{sat}}$	$C_{1,\mathrm{crit}}^{\rho\Delta\rho}$	$\rho_{\mathrm{crit}}/\rho_{\mathrm{sat}}$
KDE0v1	[29]	11.498	2.39	30.8(1)	1.18
LNS	[30]	33.750	1.25*	28.5(1)	1.35*
NRAPRii	[31]	16.599	4.21	33.1(1)	1.67*
SQMC700	[32]	15.884	4.77	31.1(1)	1.45*
SkM*	[33]	17.109	2.94	32.7(2)	1.36*
SLy5	[34]	16.375	1.72	31.7(2)	1.08
T11	[35]	14.252	1.92	31.6(2)	1.08
T44	[35]	−4.300	6.63	31.8(2)	1.05
UNEDF0	[36]	−55.623	4.13	29.0(1)	1.02*

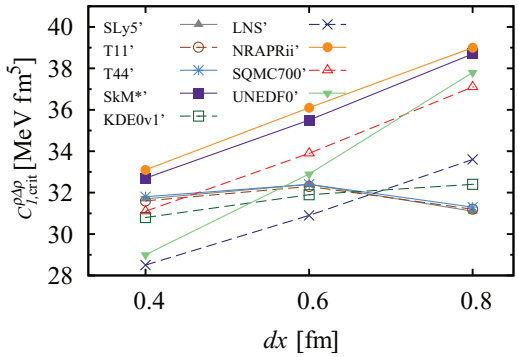

FIG. 4. (Color online) $C^{\rho\Delta\rho}_{1,\mathrm{crit}}$ obtained for ^{40}Ca with the EV8 code for the various (modified) parametrizations as a function of the step size dx.

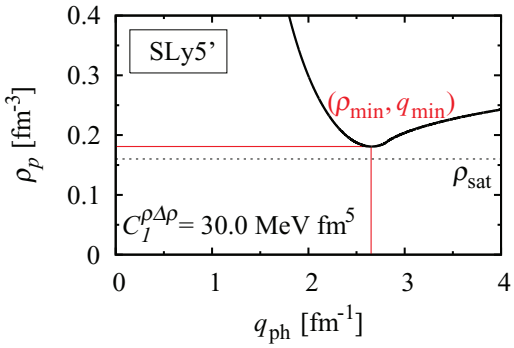

FIG. 5. (Color online) The function $\rho_p(q_{\mathrm{ph}})$ for a SLy5′ parametrization corresponding to $C_1^{\rho\Delta\rho} = 30.0$ MeV fm^5. The minimum of the $\rho_p(q_{\mathrm{ph}})$ defines the lowest density ρ_{min} at which a pole occurs for this value of $C_1^{\rho\Delta\rho}$.

^{50}Ca for which $E_1^{\rho\Delta\rho}$ is nonzero ($\sim 10^{-1}$ MeV). The code is then run for 4000 iterations. Parametrizations are considered stable when the linear slope with which $E_1^{\rho\Delta\rho}$ changes in log scale after 1000 iterations is negative (see Fig. 3) and $E_1^{\rho\Delta\rho}$ is at most of the order 10^{-10} MeV. This allows us to pin down $C^{\rho\Delta\rho}_{1,\mathrm{crit}}$ with a numerical uncertainty of about 0.2 MeV fm^5 (see Table II for $dx = 0.4$ fm). Figure 4 illustrates the sensitivity of $C^{\rho\Delta\rho}_{1,\mathrm{crit}}$ to the mesh size for the nine parametrizations under study. One observes a large change with dx for LNS′, NRAPRii′, SQMC700′, SkM*′, and UNEDF0′, whereas that variation is much milder for KDE0v1′, SLy5′, T11′, and T44′. While $C^{\rho\Delta\rho}_{1,\mathrm{crit}}$ varies over a range similar to its numerical uncertainty for the latter group, it continues to decrease linearly for the former group as one lowers the mesh to $dx = 0.4$ fm, which is half of the value typically used in nuclear structure studies. The same effect is observed for the results obtained with HOSPHE and LENTEUR, as can be seen from Fig. 2 for SLy5′ and LNS′.

A few comments are in order before the further presentation of our results. First, we have verified that pairing correlations do not alter the outcome of the analysis. Second, we note that the number of iterations necessary for the unambiguous identification of the instability is significantly larger than what is routinely used. It is thus easy to overlook the unstable nature of a given parametrization [8]. The same is true when imposing overly restrictive symmetries. As such, the values of $C^{\rho\Delta\rho}_{1,\mathrm{crit}}$ extracted with EV8 should be seen as upper bounds, as one cannot rule out that a completely symmetry-unrestricted numerical representation might result in even lower values. Last but not least, overly restrictive numerical parameters may also hide the instability as already mentioned for the code employing a HO basis expansion.

B. Connection with RPA in SNM

We now proceed to step 3 of our protocol (see Sec. II B) and aim to establish a connection between the nonconvergence occurring in calculations of finite nuclei with results obtained using the RPA in SNM.

In Fig. 5, we display a representative RPA calculation of $\rho_p(q_{\mathrm{ph}})$. The parametrization SLy5′ has been used for a value of $C_1^{\rho\Delta\rho}$ slightly below $C^{\rho\Delta\rho}_{1,\mathrm{crit}}$. The value of ρ_{min} is defined as the minimum of $\rho_p(q_{\mathrm{ph}})$ and corresponds to a momentum transfer $q_{\mathrm{ph}} = q_{\mathrm{min}}$. Its dependence on $C_1^{\rho\Delta\rho}$ is illustrated in Fig. 6 and the critical density ρ_{crit} is extracted as the value of ρ_{min} obtained for $C_1^{\rho\Delta\rho} = C^{\rho\Delta\rho}_{1,\mathrm{crit}}$. However, one has to check that a lower value of ρ_{min} is not obtained for very large values of the momentum transfer. This is illustrated in Figs. 7 and 8 which provide the same information as Fig. 5 for the nine parametrizations but extended to much larger values of q_{ph}. In Fig. 7, $C_1^{\rho\Delta\rho}$ was taken at its nominal value. All curves present a well defined minimum at a small q_{ph}, except for LNS, where $\rho_p(q_{\mathrm{ph}})$ decreases monotonically above $q_{\mathrm{ph}} = 4$ fm^{-1}. This different behavior of the LNS curve can be attributed to the fact that LNS is already unstable at the nominal value of $C_1^{\rho\Delta\rho}$. In Fig. 8, $C_1^{\rho\Delta\rho}$ was chosen at its critical value. For all EDFs, ρ_{min} is significantly reduced as compared to Fig. 7. For the four parametrizations (KDE0v1′, SLy5′, T11′, and T44′) with small error bars in $\rho_{\mathrm{crit}}/\rho_{\mathrm{sat}}$, this minimal value corresponds to a well defined minimum beyond which the curve increases in a monotonic way. By contrast, for the other five parametrizations (LNS′, SQMC700′, SkM*′, UNEDF0′, NRAPRii′), there is a monotonic decrease of the density corresponding to the

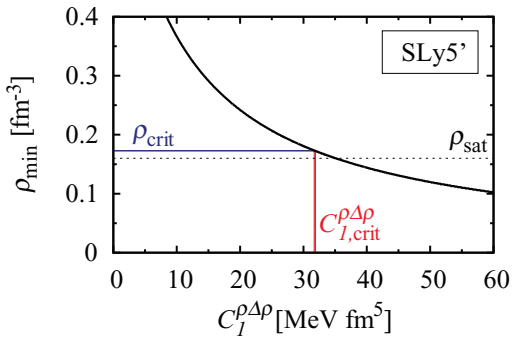

FIG. 6. (Color online) ρ_{min} as defined in Fig. 5 as a function of $C_1^{\rho\Delta\rho}$. The vertical band $C^{\rho\Delta\rho}_{1,\mathrm{crit}}$ intersects the curve to define the horizontal band ρ_{crit}. The dashed line denotes the saturation density ρ_{sat} of SNM corresponding to SLy5′.

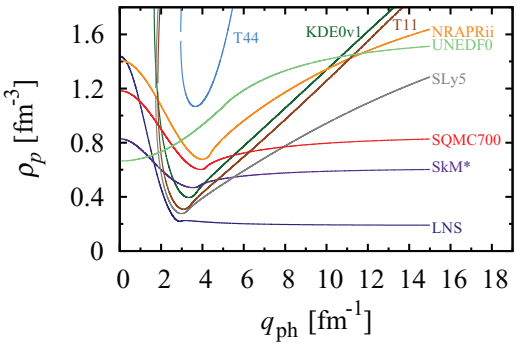

FIG. 7. (Color online) $\rho_p(q_{\rm ph})$ for the parametrizations given in Table II at the nominal value of the coupling constant $C_1^{\rho\Delta\rho}$.

pole for large values of $q_{\rm ph}$ which seemingly approaches an asymptotic value. Then, the value of ρ_p at $q_{\rm ph} = 15$ fm^{-1} is chosen as an upper bound for $\rho_{\rm min}$.

The values of $\rho_{\rm crit}$ thus extracted for the nine EDF parametrizations are listed in Table II and plotted in Fig. 9. The uncertainty on $\rho_{\rm crit}$ is estimated from that on $C_{1,\rm crit}^{\rho\Delta\rho}$, combining both the uncertainty found at a certain dx and the overall dx dependence of the results. Figure 9 also presents the interval between $\rho_{\rm sat}$ and $\rho_{\rm cent}$, which is the highest density attained in ^{40}Ca. Note that $\rho_{\rm cent}$ is typically about 20 % larger than $\rho_{\rm sat}$.

Naively, $\rho_{\rm crit}$ is expected at values of the density that are explored in a nucleus; stated differently, one would expect $\rho_{\rm crit} \leqslant \rho_{\rm cent}$. This is the case for UNEDF0, KDE0v1, SLy5, T11, and T44 over the whole uncertainty band. By contrast, for LNS, SQMC700, and SkM* it is only true at the lowest accuracies (thus, corresponding to the largest mesh size dx). With NRAPRii, $\rho_{\rm crit}$ even corresponds to densities that are never probed inside a nucleus. Clearly, the picture is more complicated than a naive one-to-one correspondence between the densities occurring in a finite nucleus and those probed by SNM. This could be expected when considering that the density at each point inside the nucleus is not behaving as if it simply were a piece of SNM with the same density. Not surprisingly, the four parametrizations (KDE0v1, SLy5, T11, and T44) for which the value of $C_{1,\rm crit}^{\rho\Delta\rho}$ does not vary much with dx (see Fig. 4) present much smaller error bars than the five others.

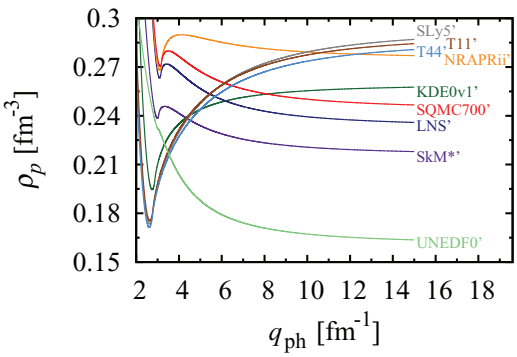

FIG. 8. (Color online) $\rho_p(q_{\rm ph})$ for the parametrizations given in Table II at the critical value of the coupling constant $C_1^{\rho\Delta\rho}$. Note the smaller scale of the y axis in comparison to Fig. 7.

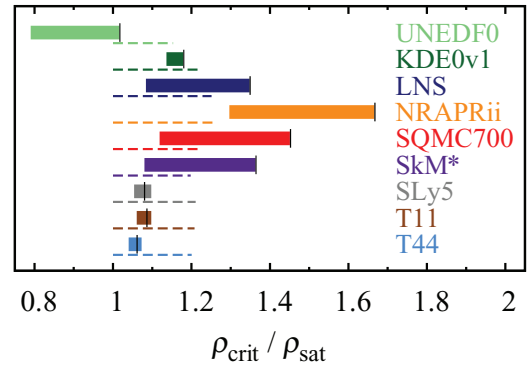

FIG. 9. (Color online) Critical density $\rho_{\rm crit}/\rho_{\rm sat}$. The uncertainty band comes both from the numerical extraction and the variation with dx. The vertical bar indicates the value for the lowest mesh size used $dx = 0.4$ fm. The dashed line indicates the interval $[1, \rho_{\rm cent}/\rho_{\rm sat}]$.

C. Discussion

Let us now look at the distribution of relative neutron momenta $f_n(q)$ in the center of ^{40}Ca, where its density is maximal. The calculation is performed in spherical symmetry with the code LENTEUR. The converged wave function for the nominal value $C_1^{\rho\Delta\rho}$ of a given parametrization is taken as a starting point of the calculation. We then set $C_1^{\rho\Delta\rho}$ to a value just above $C_{1,\rm crit}^{\rho\Delta\rho}$ and run the calculation for several hundreds of iterations. Figures 10 and 11 display $f_n^2(q)$ at various numbers of iterations on the way to the nonconvergence for SLy5′ and SQMC700′, respectively.

Both parametrizations display a very different behavior. For SLy5′, $f_n^2(q)$ starts to grow around $q = 2.2$ fm^{-1} (see Fig. 7) and increases significantly at low q values during the iterations (note the logarithmic scale). This indicates that the divergence is highly dominated by these low q values and is consistent with the fact that $\rho_p(q_{\rm ph})$ exhibits a clear global minimum at

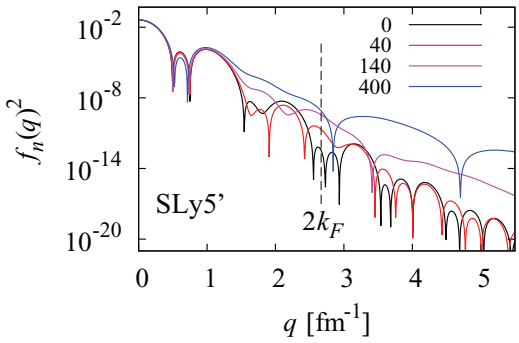

FIG. 10. (Color online) Square of the relative momentum distribution $f_n^2(q)$ at $R = 0$ for neutrons in ^{40}Ca with SLy5′ taking $C_1^{\rho\Delta\rho}$ slightly above $C_{1,\rm crit}^{\rho\Delta\rho}$. The four curves (see text) correspond to different numbers of Hartree-Fock iterations and the vertical dashed line indicates $q = 2k_F$.

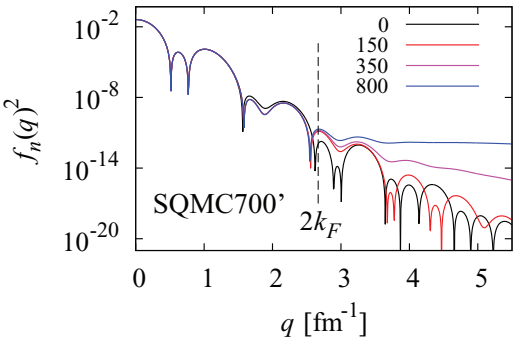

FIG. 11. (Color online) Same as Fig. 10 but for SQMC700′ ($C_1^{\rho\Delta\rho}$ slightly above $C_{1,\mathrm{crit}}^{\rho\Delta\rho}$).

small q_{ph} for SLy5′. For SQMC700′, there is only an increase of $f_n^2(q)$ for high q values. Indeed, when the calculation starts to diverge, all the weights of momenta larger than $q = 3.1$ fm^{-1} increase. This seems to be consistent with $\rho_p(q_{\mathrm{ph}})$ being a monotonously decreasing function for q_{ph} tending to ∞, without a distinct global minimum.

The observations made above for SLy5′ (SQMC700′) are valid for any parametrization belonging to the first (second) group (as defined in Sec. III B). Hence, the very different behavior of $f_n^2(q)$ at the onset of and during the divergence seems to support the hypothesis that there is a direct link between the q_{min} in SNM and the onset of instabilities in finite nuclei.

IV. CONCLUSIONS

The present study aimed at relating instabilities in energy density functional calculations of nuclei to finite-wavelength instabilities of homogeneous symmetric nuclear matter computed at the RPA level. A detailed study of the various numerical aspects in finite nuclei and of the relation between results in SNM and finite nuclei has lead us to the following conclusions:

(1) Instabilities of finite nuclei can be artificially hidden when using inappropriate numerical schemes, such as an insufficiently large basis, a too coarse mesh, or overly restrictive, e.g., spherical, symmetries. An unusually high accuracy of the calculation is required for the unambiguous detection of instabilities. Also, a code breaking spherical symmetry and relying on the discretization of a 3D mesh appears to be better fit for this task.

(2) Choosing too coarse a numerical representation to numerically hide a finite-size instability is not equivalent to suppressing it. Although a seemingly converged solution of the self-consistent mean-field equations might be found for a given set of numerical parameters, the observables remain strongly dependent on the choices made for these parameters.

(3) Omitting the UNEDF0 parametrization for the moment, the parametrizations studied can be systematically classified in two groups. The first one (SLy5, KDE0v1, T11, T44) corresponds to parametrizations for which the uncertainty in $C_{1,\mathrm{crit}}^{\rho\Delta\rho}$ is small and $\rho_p(q_{\mathrm{ph}})$ has a marked absolute minimum as a function of q_{ph}. The behavior of $f_n^2(q)$ indicates that the divergence is dominated by low q values. For this group of parametrizations, ρ_{crit} within error bars is smaller than ρ_{cent}. For the second group (LNS, NRAPRii, SQMC700, SkM*), the uncertainty in $C_{1,\mathrm{crit}}^{\rho\Delta\rho}$ is large, $\rho_p(q_{\mathrm{ph}})$ is monotonously decreasing beyond $q_{\mathrm{ph}} \approx 3$ fm^{-1}, and $f_n^2(q)$ grows predominantly for large q values when the calculations diverge.

(4) The same grouping of the parametrizations is observed when considering the quality of their prediction of nuclear masses. SLy5, T44, T11, and KDE0v1 were adjusted treating properties of nuclear matter and finite nuclei on similar footing. By contrast, no data on nuclear masses were included in the protocol for LNS and SQMC700. As already pointed out in the original references, the mass residuals for these parametrizations are prohibitively large (>5%). NRAPR was adjusted in a similar manner, with only the spin-orbit part of the EDF being tuned to the binding energies of ^{208}Pb, ^{90}Zr, and ^{40}Ca, but with very poor results. Finally, SkM* has been constructed using a semiclassical approximation of the mean field and also leads to nonsatisfactory results for binding energies.

(5) Finally, let us consider UNEDF0. It has a large uncertainty in $C_{1,\mathrm{crit}}^{\rho\Delta\rho}$ and a $\rho_p(q_{\mathrm{ph}})$ that decreases systematically with q_{ph}, hence placing it in the second group of parametrizations. However, $\rho_{\mathrm{crit}} < \rho_{\mathrm{cent}}$ and properties of nuclear matter and finite nuclei were treated on equal footing during its adjustment, thus associating it with the first group of parametrizations. We do not see a clear explanation for this mixed behavior. One can, however, note that the value found for $C_{1,\mathrm{crit}}^{\rho\Delta\rho}$ is far from its nominal value, even if it falls within the error bars reported in [36].

Combining all aspects of the study carried out in the present article, no universal quantitative picture emerges regarding the value of ρ_{crit} when scanning various Skyrme parametrizations. Omitting UNEDF0, which has a large uncertainty in ρ_{crit} and for which $C_{1,\mathrm{crit}}^{\rho\Delta\rho}$ is far from its nominal value, one finds a group of parametrizations (SLy5, KDE0v1, T11, T44) that delivers a high quality prediction of nuclear masses and for which the ρ_{crit} determined by means of RPA for SNM corresponds to densities that are probed in a finite nucleus. On the other hand, one finds a group of parametrizations (LNS, NRAPRii, SQMC700, SkM*) that lead to less satisfactory results in the description of nuclear masses and for which there seems to be no easy one-to-one correspondence between ρ_{crit} and the densities probed in a nucleus. Note, however, that LNS, NRAPRii, and SQMC700 are shown to be consistent with a large set of pseudodata in SNM.

For the purpose of constructing parametrizations for the description of finite nuclei that are stable with respect to scalar-isovector perturbations, we propose a twofold criterion. First the minimum of $\rho_p(q_{\mathrm{ph}})$ should be larger than the central

density in ^{40}Ca, in practice around 1.2 times the saturation density. In addition, one also has to verify that $\rho_p(q_{\rm ph})$ exhibits a distinct global minimum and is not a monotonously decreasing function for large transferred momenta.

Since RPA calculations of SNM can be performed at no computational cost, the above stability criterion can be easily incorporated in fitting protocols to identify and reject (near-) unstable regions of the parameter space when adjusting the coefficients of the EDF. The value of this threshold should of course be increased if one is interested in nuclear systems exploring densities higher than those encountered in nuclear ground states, such as they appear in neutron stars for example.

ACKNOWLEDGMENTS

M.B. and K.B. thank P.-G. Reinhard for a clarifying discussion about the RPA in infinite matter. This work was supported by the Agence Nationale de la Recherche under Grant No. ANR 2010 BLANC 0407 "NESQ", by the CNRS/IN2P3 through the PICS No. 5994, by the European Union's Seventh Framework Programme ENSAR under grant agreement n262010, by the Belgian Office for Scientific Policy under Grant No. PAI-P7-12, and by the Academy of Finland and University of Jyväskylä within the FIDIPRO program. V.H. acknowledges financial support from the F.R.S.-FNRS Belgium.

[1] M. Bender, P.-H. Heenen, and P.-G. Reinhard, Rev. Mod. Phys. **75**, 121 (2003).
[2] S. Stringari and J. Treiner, Phys. Rev. B **36**, 8369 (1987).
[3] M. Barranco, R. Guardiola, S. Hernańdez, R. Mayol, J. Navarro, and M. Pi, J. Low Temp. Phys. **142**, 1 (2006).
[4] S. Stringari and J. Treiner, J. Chem. Phys. A **87**, 5021 (1987).
[5] S. Weisgerber and P.-G. Reinhard, Z. Phys. D **23**, 275 (1992).
[6] A. Bulgac and M. Forbes, Phys. Rev. Lett. **101**, 215301 (2008).
[7] F. Tondeur, M. Brack, M. Farine, and J. M. Pearson, Nucl. Phys. A **420**, 297 (1984).
[8] T. Lesinski, K. Bennaceur, T. Duguet, and J. Meyer, Phys. Rev. C **74**, 044315 (2006).
[9] N. Schunck, J. Dobaczewski, J. McDonnell, J. Moré, W. Nazarewicz, J. Sarich, and M. V. Stoitsov, Phys. Rev. C **81**, 024316 (2010).
[10] V. Hellemans, P.-H. Heenen, and M. Bender, Phys. Rev. C **85**, 014326 (2012).
[11] A. B. Midgal, *Theory of Finite Fermi Systems and Applications to Atomic Nuclei* (Wiley, New York, 1967).
[12] J. Navarro and A. Polls, Phys. Rev. C **87**, 044329 (2013).
[13] I. Vidaña and I. Bombaci, Phys. Rev. C **66**, 045801 (2002).
[14] I. Bombaci, A. Polls, A. Ramos, A. Rios, and I. Vidaña, Phys. Lett. B **632**, 638 (2006).
[15] C. García-Recio, J. Navarro, N. Van Giai, and N. N. Salcedo, Ann. Phys. (NY) **214**, 293 (1992).
[16] J. Margueron, J. Navarro, and N. Van Giai, Phys. Rev. C **74**, 015805 (2006).
[17] D. Davesne, M. Martini, K. Bennaceur, and J. Meyer, Phys. Rev. C **80**, 024314 (2009); **84**, 059904(E) (2011).
[18] A. Pastore, D. Davesne, Y. Lallouet, M. Martini, K. Bennaceur, and J. Meyer, Phys. Rev. C **85**, 054317 (2012).
[19] C. Ducoin, J. Margueron, and Ph. Chomaz, Nucl. Phys. A **809**, 30 (2008).
[20] C. Ducoin, C. Providência, A. M. Santos, L. Brito, and Ph. Chomaz, Phys. Rev. C **78**, 055801 (2008).
[21] C. Ducoin, Ph. Chomaz, and F. Gulminelli, Nucl. Phys. A **789**, 403 (2007).
[22] M. Kortelainen and T. Lesinski, J. Phys. G **37**, 064039 (2010).
[23] A. Sulaksono, Kasmudin, T. J. Bürvenich, P.-G. Reinhard, and J. A. Maruhn, Int. J. Mod. Phys. E **20**, 81 (2011).
[24] B. Friman and P. Henning, Phys. Lett. B **206**, 579 (1988).
[25] H.-G. Döbereiner and P.-G. Reinhard, Phys. Lett. B **227**, 305 (1989).
[26] K. J. Pototzky, J. Erler, P.-G. Reinhard, and V. O. Nesterenko, Eur. J. Phys. A **46**, 299 (2010).
[27] P. D. Stevenson, P. M. Goddard, J. R. Stone, and M. Dutra, AIP Conf. Proc. **1529**, 262 (2013).
[28] M. Dutra, O. Lourenço, J. S. Sá Martins, A. Delfino, J. R. Stone, and P. D. Stevenson, Phys. Rev. C **85**, 035201 (2012).
[29] B. K. Agrawal, S. Shlomo, and V. K. Au, Phys. Rev. C **72**, 014310 (2005).
[30] L. G. Cao, U. Lombardo, C. W. Shen, and N. Van Giai, Phys. Rev. C **73**, 014313 (2006).
[31] A. W. Steiner, M. Prakash, J. M. Lattimer, and P. J. Ellis, Phys. Rep. **411**, 325 (2005).
[32] P. A. M. Guichon, H. H. Matevosyan, N. Sandulescu, and A. W. Thomas, Nucl. Phys. A **772**, 1 (2006).
[33] J. Bartel, P. Quentin, M. Brack, C. Guet, and H.-B. Håkansson, Nucl. Phys. A **386**, 79 (1982).
[34] E. Chabanat, P. Bonche, P. Haensel, J. Meyer, and R. Schaeffer, Nucl. Phys. A **635**, 231 (1998).
[35] T. Lesinski, M. Bender, K. Bennaceur, T. Duguet, and J. Meyer, Phys. Rev. C **76**, 014312 (2007).
[36] M. Kortelainen, T. Lesinski, J. Moré, W. Nazarewicz, J. Sarich, N. Schunck, M. V. Stoitsov, and S. Wild, Phys. Rev. C **82**, 024313 (2010).
[37] B. G. Carlsson, J. Dobaczewski, and M. Kortelainen, Phys. Rev. C **78**, 044326 (2008).
[38] M. Stoitsov, M. Kortelainen, S. K. Bogner, T. Duguet, R. J. Furnstahl, B. Gebremariam, and N. Schunck, Phys. Rev. C **82**, 054307 (2010).
[39] J. Sadoudi, T. Duguet, J. Meyer, and M. Bender, Phys. Rev. C (to be published), arXiv:1310.0854.
[40] A. Pastore, D. Davesne, K. Bennaceur, J. Meyer, and V. Hellemans, Phys. Scr., T **154**, 014014 (2013).
[41] M. Casas, J. Martorell, E. Moya de Guerra, and J. Treiner, Nucl. Phys. A **473**, 429 (1987).
[42] B. Carlsson, J. Dobaczewski, J. Toivanen, and P. Vesely, Comput. Phys. Commun. **181**, 1641 (2010).
[43] K. Bennaceur (unpublished).
[44] P. Bonche, H. Flocard, and P.-H. Heenen, Comput. Phys. Commun. **171**, 49 (2005).